ACS Catalysis

Research Article

pubs.acs.org/acscatalysis

Metal Nanoparticle/Carbon Quantum Dot Composite as a Photocatalyst for High-Efficiency Cyclohexane Oxidation

Ruihua Liu,[†] Hui Huang,[†] Haitao Li,[†] Yang Liu,*[,†] Jun Zhong,[†] Youyong Li,[†] Shuo Zhang,[‡] and Zhenhui Kang*[,†]

[†]Institute of Functional Nano and Soft Materials (FUNSOM) & Jiangsu Key Laboratory for Carbon-Based Functional Materials and Devices, Soochow University, Suzhou, People's Republic of China

[‡]Shanghai Synchrotron Radiation Facility, Shanghai Institute of Applied Physics, Chinese Academy of Science, Shanghai, People's Republic of China

Supporting Information

ABSTRACT: High-efficiency and high-selectivity catalytic oxidation of alkanes under mild conditions is a major objective of current catalysis chemistry and chemical production. Despite extensive development efforts on new catalysts for cyclohexane oxidation, current commercial processes still suffer from low conversion, poor selectivity, and excessive production of waste. We demonstrate the design and synthesis of composites made from metal nanoparticles and carbon quantum dots (CQDs) for high-efficiency and high-selectivity photocatalyst systems for the green oxidation of cyclohexane. Remarkably, the present Au nanoparticles/CQDs composite photocatalyst yields 63.8% conversion efficiency and 99.9% selectivity for the green oxidation of cyclohexane to cyclohexanone, using H_2O_2 under visible light at room temperature. Given its diversity and versatility of structural and composition design, metal nanoparticles/CQDs composites may provide a powerful pathway for the development of high-performance catalysts and production processes for green chemical industry.

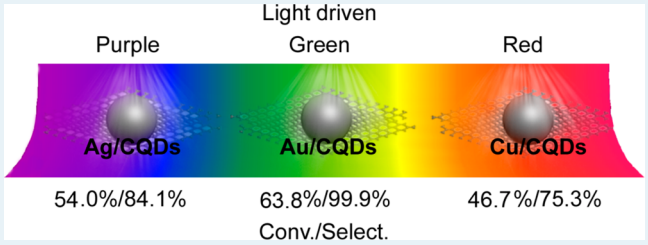

KEYWORDS: *carbon quantum dots, composites, cyclohexane oxidation, photocatalysis, selective oxidation*

INTRODUCTION

One of the principal objectives of catalysis chemistry in the 21st century is the high-efficiency and high-selectivity catalytic oxidation of alkanes,[1] especially cyclohexane oxidation under mild conditions.[2] However, the high activation energy of C−H bond breaking in cyclohexane dictates harsh reaction conditions, i.e., high temperature and high pressure.[3] Apart from its intrinsic importance in the chemistry of C−H activation, the selective oxidation of cyclohexane to cyclohexanone and cyclohexanol (~10^6 tons/yr) is the key step of the commercial production of nylon-6 and nylon-66 polymers. Despite extensive development efforts for cyclohexane oxidization catalysts, today's commercial processes still suffer from high temperature (150−160 °C), high pressure (1−2 MPa), low yield (<15%), low selectivity (<80%), and excessive production of waste.[4,5] Catalysts enabling cyclohexane oxidation under mild conditions (below the boiling point of cyclohexane, 80.7 °C) would alleviate the potential hazard of harsh reaction conditions, as well as allow for more selective and controlled reactions. As a preferred oxidant in liquid phase, hydrogen peroxide can work at low temperature, produces only water as a byproduct, and has a high oxygen uptake (47%).[6−8] However, cyclohexane oxidation with H_2O_2 at low temperature using the current catalysts (such as weak acid resin,[9] iron bispidine complexes,[10] Ru complex,[11] Cr/Ti/Si oxides,[12] Na-GeX,[13] mesoporous TS-1,[14] Ti-MCM-41,[15] metal aluminophosphates,[16] biomimetic systems,[17] and Cu−Cr_2O_3[18]) invariably suffers from large amount of organic solvent (i.e., acetone and acetonitrile), poor selectivity, and low H_2O_2 efficiency, thus making its industrialization difficult.

Carbon quantum dots (CQDs) with richly fluorescent and photoelectrochemical properties[19,20] can serve as either photoinduced electron acceptors or donors.[20] They can function not only as an efficient photocatalyst (for highly selective oxidation), but also as a multifunctional component in photocatalyst design[21] to promote wider spectrum absorption and separation of electrons and holes, as well as to stabilize photolysis semiconductors. Metal nanoparticles (Au, Cu, etc.) are known to possess catalytic activities for selective oxidation reactions.[22,23] In addition, surface plasma resonance absorption can also induce good photocatalytic abilities of metal nanoparticles (Au, Ag, etc.).[24,25] Here, we report the design of a tunable photocatalyst based on the composite of CQDs and metal nanoparticles for the selective oxidation of cyclohexane. Significantly, the Au nanoparticles/CQDs (Au/CQDs) composite catalyst yielded oxidation of cyclohexane to cyclohexanone

Received: October 11, 2013
Revised: November 19, 2013
Published: December 11, 2013

with 63.8% efficiency and >99.9% selectivity in the presence of H_2O_2 under visible light at room temperature (see Scheme 1).

Scheme 1. Au/CQDs Composites as a Photocatalyst for Selective Oxidation of Cyclohexane in the Presence of H_2O_2 under Visible Light

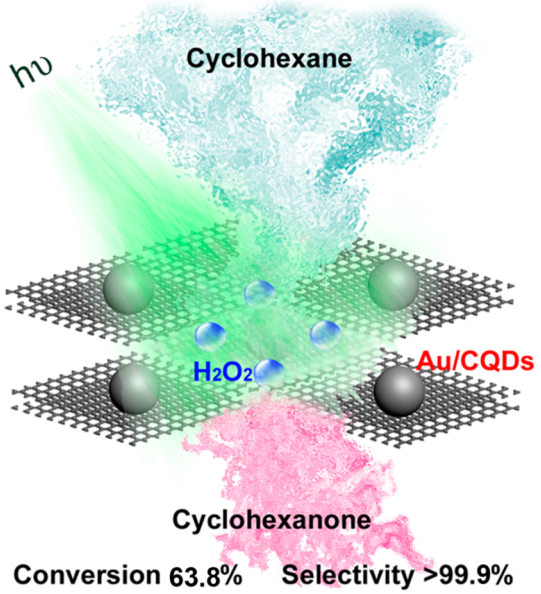

RESULTS AND DISCUSSION

Characterization of Au/CQDs Composites. The CQDs were synthesized through a method of electrochemical ablation of graphite. As shown in Figure S1 in the Supporting Information, the surface functional groups on the CQDs are hydroxyl (−OH), carboxy (C═O), and epoxide/either (C−O−C). For the present composite catalyst, the interaction between the p/π orbitals of C and d orbitals of Au in AuNPs, and the interactions between the functional groups on the CQDs (−OH, C═C, C═O) and the AuNPs are responsible for the formation and the high stability of the Au/CQDs composite catalyst. Au/CQDs composites were synthesized by dropwise addition of $HAuCl_4$ solution to CQDs solution with vigorously magnetic stirring in darkness at room temperature (see the Experimental Section for details). Figure 1a shows the transmission electron microscopy (TEM) image of the spherical and well-dispersed Au/CQDs composites with sizes of 5−15 nm. The upper inset in Figure 1a is the energy-dispersive X-ray (EDX) spectrum of Au/CQDs composites, where the Cu peaks are from the copper TEM grid, Au peaks from AuNPs, O and C peaks from CQDs, and amorphous carbon film on the Cu grid. X-ray diffraction (XRD) pattern is shown in the lower inset in Figure 1a. All the characteristic diffraction peaks marked by a white inverted triangle (▽) can be readily indexed to (111), (200), (220), (311), and (222) planes of metallic Au (JCPDS File Card No. 1-1172), respectively. The broad diffraction peak at 26° (marked by a white diamond (◇)) is the characteristic peak of carbon. The high-resolution TEM image (HRTEM) of Au/CQDs composites is shown in Figure 1b. Clear lattice spacings of 0.240 and 0.235 nm are in well agreement with the (100) crystallographic planes of graphitic carbon and (111) planes of crystalline Au, respectively. Compared with that of CQDs or AuNPs, the UV−visible absorption spectrum of Au/CQDs composites displays typical absorbance in both UV and visible regions. In Figure 1c, the absorption peak

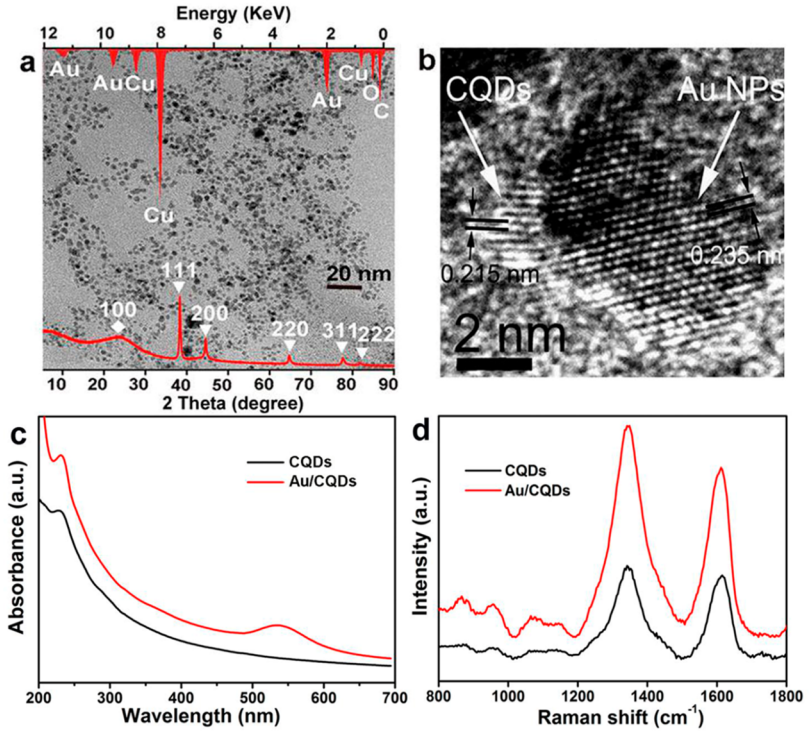

Figure 1. (a) Transmission electron microscopy (TEM) image, X-ray diffraction (XRD) pattern (shown as the red overlay at the top portion of the panel) and energy-dispersive X-ray (EDX) spectrum (shown as the red overlay at the bottom portion of the panel) of Au/CQDs composites; (b) high-resolution transmission electron microscopy (HRTEM) image of Au/CQDs composites; (c) ultraviolet−visible light (UV-vis) absorbance spectrum of CQDs and Au/CQDs; and (d) typical Raman spectra of CQDs and Au/CQDs composites.

dx.doi.org/10.1021/cs400913h | ACS Catal. 2014, 4, 328−336

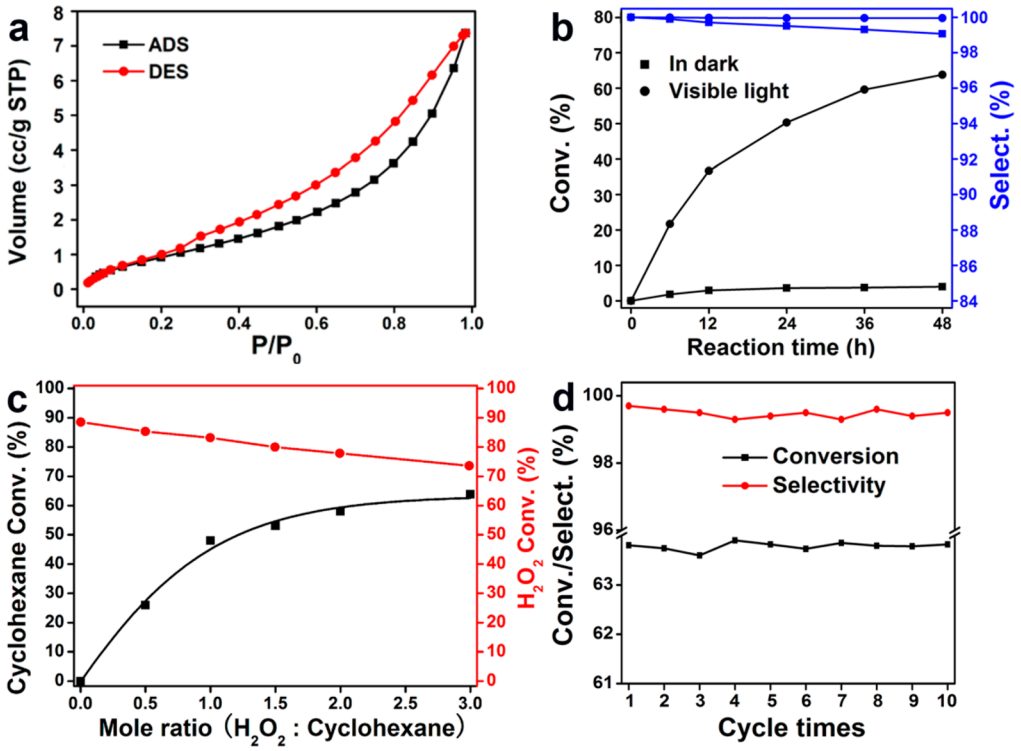

Figure 2. (a) Cyclohexane adsorption−desorption isotherm curves of Au/CQDs composites; (b) time dependence of conversion efficiency and selectivity of cyclohexane oxidation were investigated in darkness and visible light (H_2O_2/cyclohexane molar ratio is 3:1); (c) the conversion of cyclohexane and H_2O_2 under different H_2O_2/cyclohexane molar ratios; (d) conversion and selectivity efficiency of the oxidation of cyclohexane on Au/CQDs composites over cycling 10 times (H_2O_2/cyclohexane molar ratio = 3:1).

at ∼230 nm represents a typical absorption of CQDs, similar to that of polycyclic aromatic hydrocarbons,[26] while the absorption peak in the visible region (490−590 nm) is attributed to the surface plasmon band of AuNPs.[27] The Raman spectrum of Au/CQDs composites in Figure 1d shows the D-band and G-band of carbon at 1343 and 1611 cm^{-1}.[28] The intensity of D-band and G-band of Au/CQDs composite is obviously higher than that of pure CQDs, which is due to the surface enhancement Raman scattering effect of AuNPs.[29]

Catalytic Oxidation of Cyclohexane Using Au/CQDs composites. The measured cyclohexane adsorption−desorption isotherm of Au/CQDs composites (Figure 2a) exhibits the type-IV curve characteristics,[30] indicating that Au/CQDs composites have good adsorption to cyclohexane. In the catalytic experiments, H_2O_2 (30%) as oxidant was added dropwise to the mixture of Au/CQDs composites (25 mg) and cyclohexane (50 mL) in a round-bottom flask (250 mL) with water condenser and continuous magnetic stirring. The oxidation products were analyzed by gas chromatography (GC) and gas chromatography−mass spectroscopy (GC-MS). Figure 2b shows the time dependence of the conversion and selectivity of cyclohexane oxidation to cyclohexanone with Au/CQDs composites as the photocatalyst driven by visible light. It reveals that conversion efficiency increases with increasing reaction time, while the selectivity to cyclohexanone is nearly constant at 99.9%, regardless of the conversion efficiency (Table 1). After 48 h reaction, a high conversion efficiency of 63.8% and high selectivity of over 99.9% were achieved concurrently. The conversion of cyclohexane and H_2O_2 under different molar ratios of H_2O_2/cyclohexane (0.0, 0.5, 1.0, 1.5, 2.0, 3.0) were also investigated and shown in Figure 2c. With the mole ratio of

Table 1. Different Catalysts for Photocatalytic Oxidation of Cyclohexane (H_2O_2/Cyclohexane Molar Ratio = 3:1)[a]

				Selectivity (%)	
entry	catalyst	oxidant	conversion (%)	cyclohexanone	$\sum_{sel}C_6$
1	none	none			
2	CQDs	H_2O_2	3.0	99.9	100
3	AuNPs	H_2O_2	5.0	98.4	100
4	CQDs and AuNPs	H_2O_2	7.0	76.5	100
5	**Au/CQDs**	**H_2O_2**	**63.8**	**>99.9**	**100**
6	Au/SiO_2	H_2O_2	30.3	54.1	100
7	Au/carbon nanotube	H_2O_2	22.1	49.7	100
8	Au/graphene	H_2O_2	23.9	50.1	100
9	Au/graphite	H_2O_2	14.2	64.2	100

[a]Reactions were carried out in a round-bottom flask. Conversion and selectivity were determined by GC analysis; the variance of values is estimated to be less than ±2%.

H_2O_2/cyclohexane increasing, the conversion of cyclohexane increases and the conversion of H_2O_2 slightly decreases.

The following experiments further highlight the effectiveness of the present composite catalyst: (1) blank reaction (i.e., without catalyst) would not produce any oxidation products (entry 1 in Table 1); (2) CQDs and AuNPs used separately as catalyst (entries 2 and 3 in Table 1) yielded cyclohexane oxidation with low conversion of only 3% and 5%, respectively; and (3) a mixture of CQDs and AuNPs as catalyst yielded slight improvement, but conversion and selectivity of cyclohexane to cyclohexanone remained low at 7.0% and 76.5%, respectively (entry 4 in Table 1). In remarkable contrast, the Au/CQDs composites catalyst shows high conversion efficiency

dx.doi.org/10.1021/cs400913h | ACS Catal. 2014, 4, 328−336

(63.8%) and high selectivity (>99.9%), which also remain nearly constant over 10 catalytic cycles (Figure 2d). After carefully analyzing the products, it was found that the selectivity of C_6 products is ~100% (see Table 1), without any CO_2 evolved. As shown in Figure 2d, the Au/CQDs are stable enough during the repeated experiments without exhibiting any significant loss of catalytic activity and selectivity. After recycling 10 times, Au/CQDs still retain high catalytic activity and selectivity of cyclohexane oxidation. Moreover, the filtrate solution test (an additional 24 h of reaction after removing the Au/CQDs composites from the reaction medium) showed no catalytic activity, indicating that leaching did not play an important role in the present system. The above experiments show Au/CQDs composites indeed function as a high-performance photocatalyst in the present reaction system.

Cyclohexane oxidation was further carried out with the Au/CQDs composites catalyst driven by light of different wavelengths (Figure 3a). Figure 3b shows that the best conversion

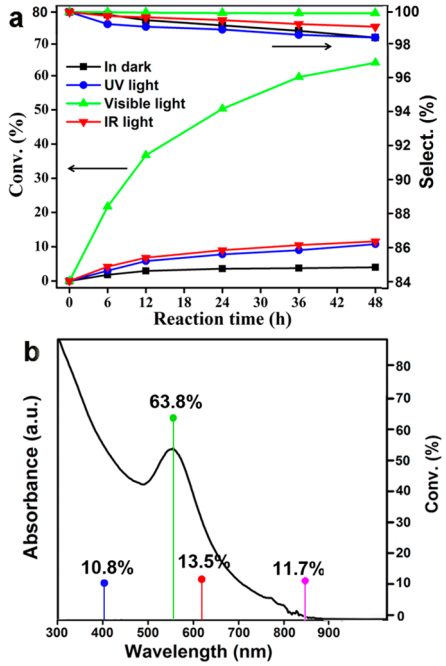

Figure 3. Time dependence of the conversion and selectivity of the oxidation of cyclohexane with Au/CQDs composites as photocatalyst (the molar ratio of H_2O_2/cyclohexane is 3:1) driven by different lighting conditions: (a) in darkness, UV light (high-pressure mercury lamp, main wavelength of λ = 365 nm), Visible light (xenon lamp with visible-CUT filter to cut off light with a wavelength of λ < 420 nm), and infrared (IR) light (xenon lamp with visible-CUT filter to cut off light with a wavelength of λ < 700 nm); (b) blue (400 nm), green (525 nm), red (620 nm), and IR (850 nm) light, using high-power (>1 W) light-emitting diodes (LEDs) as light sources.

efficiency was obtained in green light, whose wavelength matches the surface plasma resonance zone of AuNPs (490−590 nm, see Figure S2 in the Supporting Information).[27] However, under the same conditions (visible light, room temperature), the use of AuNPs supported on SiO_2 spheres (Au/SiO_2 nanospheres; TEM and HRTEM images, see Figure S3 in the Supporting Information) as catalyst only yielded a low conversion efficiency of 30.3% and a low selectivity of 54.1% for cyclohexanone (entry 6 in Table 1). However, other carbon-based catalysts (such as Au/carbon nanotubes, Au/graphite, and Au/graphene) also could not get good photocatalytic abilities upon the oxidation of cyclohexane (entries 7, 8, and 9 in Table 1). The totality of the experiments shows that the high conversion and selectivity in the present photocatalyst system should be attributed to the collective contribution and interactions of CQDs and AuNPs.

Interaction between AuNPs and CQDs. X-ray absorption spectroscopy (XAS, element-specific spectroscopic technique for structural information of different species) experiments were performed to investigate the electronic structure of Au/CQDs composites.[31] Au L_3-edge (X-ray absorption near edge structure, XANES) and extended X-ray absorption fine structure (EXAFS) data for Au/CQDs composites with and without visible light irradiation were collected. The XANES data are shown in Figure 4a, and the Fourier transform of the

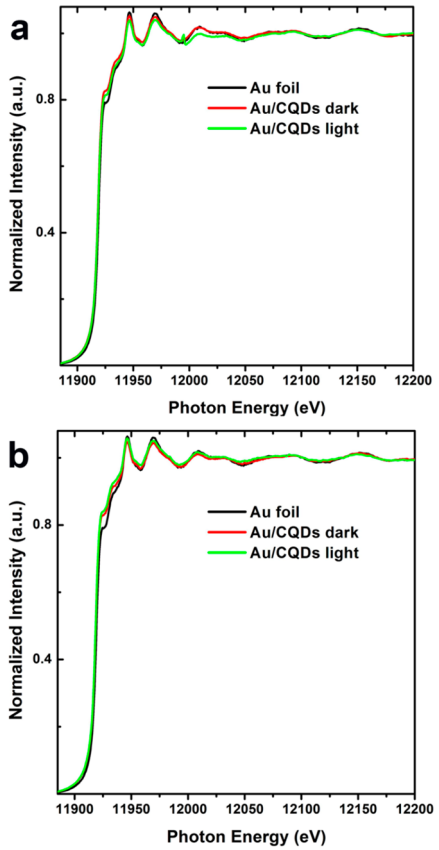

Figure 4. (a) Au L_3-edge XANES spectra of Au/CQDs composites with and without visible light irradiation. (b) Au L_3-edge XANES spectra of Au/CQDs composites with and without visible light irradiation under in situ reaction condition.

EXAFS data in R-space shown in Figure 5a. The XANES data for Au/CQDs composites with and without visible-light irradiation also show very similar spectral shape. In contrast, obvious differences between light-on and light-off can be found in the Fourier transform of the EXAFS data in the R-space. The main peak at ~2.6 Å can be attributed to Au−Au bonds. Au/CQDs composites before light irradiation show a main peak at 2.6 Å, indicating the existence of AuNPs, and the peak intensity is lower than that for Au foil revealing the nature of AuNPs.[32] Strikingly, when the same Au/CQDs composites were exposed to visible light, a new peak at 1.5 Å can be observed. This peak could be attributed to the interaction between CQDs and

dx.doi.org/10.1021/cs400913h | ACS Catal. 2014, 4, 328−336

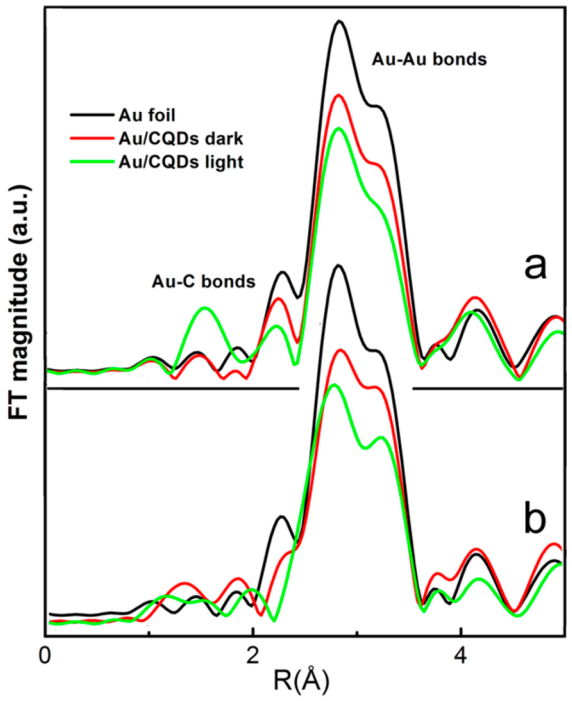

Figure 5. (a) Fourier transform of the Au/CQDs composites EXAFS data in R-space with and without light. (b) Fourier transform of the Au/CQDs composites EXAFS data in R-space with and without light under in situ reaction condition. The spectrum of Au foil is also shown for comparison.

AuNPs, such as Au−C bonds.[32] Also, a further decrease of the main peak intensity can be observed, suggesting a decrease of Au−Au bonds with the formation of Au−C bonds. In the following experiments, Au L_3-edge XANES and EXAFS data for Au/CQDs composites were collected during the in situ photocatalytic reaction. Under the in situ reaction condition, the XANES data for Au/CQDs composites (Figure 4b) is also very similar to that for Au NPs and Au foil. However, as shown in Figure 5b, under the in situ reaction condition, there is no obvious signal on the formation of Au−C bonds between CQDs and AuNPs, even if a further decrease of the main peak (2.6 Å) intensity can be observed under visible light. The disappearing of the Au−C bonds signal further confirms that the photocatalytic reaction is really occurred on the interface of AuNPs and the CQDs.

In the followed experiments, the photoinduced electron transfer properties of CQDs irradiated by visible light were investigated. It was found that the photoluminescence (PL) of CQDs excited by 485 nm with emission located at 550 nm could be quenched by either electron acceptor or electron donor molecules in solution, confirming that CQDs are excellent as both electron donors and acceptors under visible light. As shown in Figures S4a and S4b in the Supporting Information, CQDs can exhibit broad luminescence peak at ∼550 nm with the excitation at 485 nm, and the emission intensities were quenched by the known electron donors (*N*,*N*-diethylaniline, DEA) and electron acceptors (2,4-dinitrotoluene). Figure S4c and S4d in the Supporting Information show the luminescence decays of CQDs with Stern−Volmer quenching constants (see the insets of Figure S4c and S4d in the Supporting Information, $Ksv = \tau_F^0 k_q$) from linear regression of 33.0 and 21.5 M^{-1}, respectively. The above results that the PL of CQDs were quenched highly efficiently by either electron acceptors or electron donors, clearly confirming that CQDs are excellent as both electron acceptors and electron donors.

To obtain the further insight about the interaction between AuNPs and CQDs, we examined the PL spectra of CQDs, AuNPs, and Au/CQDs (Figure 6a). It indicated that the PL of CQDs is effectively quenched in the Au/CQDs system. The corresponding PL lifetime of Au/CQDs shown in Figure 6b decreased to 1.5 ns, from 4.0 ns for pure aqueous CQDs solution. It demonstrates the dynamic PL quenching in the Au/CQDs system is attributed to an ultrafast electron transfer process in the Au/CQDs system.

Proposed Mechanism Study. The electrocatalytic ability of Au/CQDs composites for H_2O_2 decomposition was examined in a conventional three-electrode electrochemical cell.[20] As shown in Figure 7a, the bare glassy carbon electrode shows no obvious electrochemical response (black curve), while the Au/CQDs-modified glassy carbon electrode exhibits obvious catalytic ability for H_2O_2 decomposition. Under visible-light irradiation, the response of Au/CQDs-modified electrode for H_2O_2 decomposition is stronger (onset potential at −0.2 V) than that without light irradiation (onset potential at −0.6 V). Further experiments show that Au/CQDs composites-modified electrodes have the highest electrocatalytic activity for H_2O_2 decomposition among various modified electrodes (CQDs, AuNPs, and their mixture), which is also consistent with the photocatalytic results in Table 1. All electrochemical experiments suggested that the visible light-promoted catalytic activity of Au/CQDs composites for H_2O_2 decomposition should play key roles for the highly catalytic activity in selective oxidation of cyclohexane.

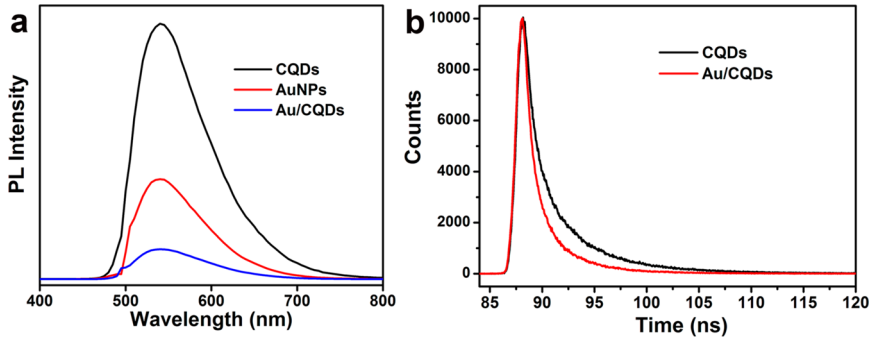

Figure 6. (a) PL spectra (485 nm excitation) of CQDs, AuNPs and Au/CQDs; (b) luminescence decays (485 nm excitation, monitored with 550 nm narrow bandpass filter) of CQDs and Au/CQDs.

dx.doi.org/10.1021/cs400913h | *ACS Catal.* 2014, 4, 328−336

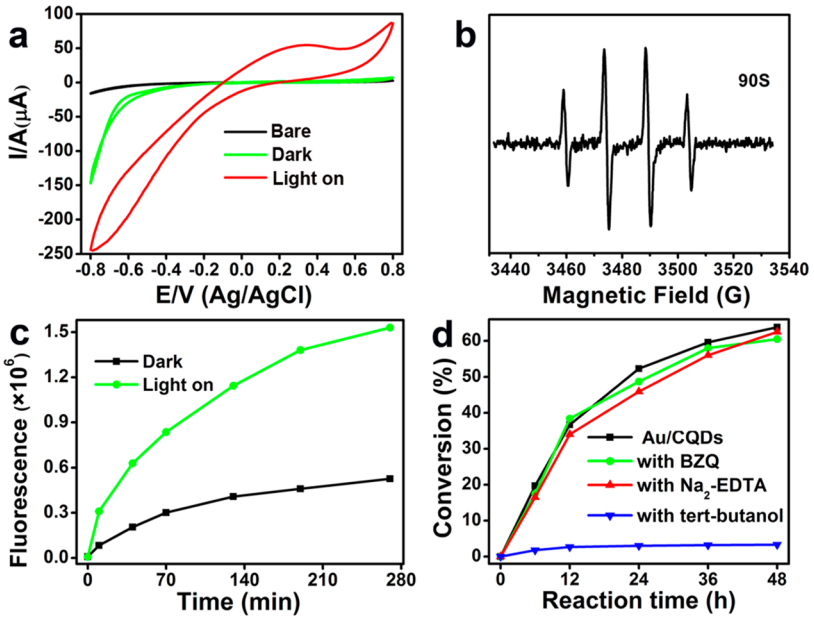

Figure 7. (a) Cyclic voltammograms of bare glassy carbon electrode and Au/CQDs-modified glassy carbon electrode in phosphate buffer (pH 7.4) and in the presence of 10 mM H_2O_2. Scan rate = 25 mV/s. A 450-W xenon lamp was used as the light source with a visible-CUT filter to cut off light with a wavelength of λ < 420 nm. (b) ESR signals of the DMPO−•OH (aqueous solution) adducts for Au/CQDs−H_2O_2 system under visible-light irradiation. [Au/CQDs] = 4 mg/50 mL; [H_2O_2] = 10 mM; [DMPO] = 40 mM. (c) Time dependence of the fluorescence intensity of the supernatant liquid of Au/CQDs composites for two different reaction conditions (in darkness and under visible light). A 450-W xenon lamp was used as the light source with a visible-CUT filter to cut off light with a wavelength of λ < 420 nm. (d) Photocatalysis activities of Au/CQDs in reactive species trapping experiments with three types of reactive species scavengers (H_2O_2/cyclohexane molar ratio = 3:1).

In general, HO• produced by decomposition of H_2O_2 is a strong oxidant, and can easily oxidize cyclohexane to cyclohexanone and cyclohexanol. Here, a spin-trapping electron spin resonance (ESR) test was carried out to check the active oxygen species produced by Au/CQDs-H_2O_2 system under visible light. As shown in Figure 7b, typical characteristic quartet peaks of DMPO−•OH (DMPO, dimethyl pyridine N-oxide) adducts appeared gradually upon light irradiation of the aqueous Au/CQDs−H_2O_2 system, which suggested that HO• is the active oxygen species in this photocatalytic oxidation process. To further confirm whether HO· is the main active oxygen specie responsible for present selective oxidative reaction, a terephthalic acid PL (TA-PL) probing assay was used to detect the amount of HO• under different reaction conditions[33] (see the Experimental Section). The reaction between the hydroxyl radicals and terephthalate yielding one intensely fluorescent monohydroxylated isomer is shown in Figure S5 in the Supporting Information. Figure 7c confirmes that, in the buffer solution containing Au/CQDs catalyst, a larger number of HO• will be produced under visible-light irradiation than that produced in darkness.

Figure 8 shows the PL intensities of the supernatant TA-PL assay solutions after removing the Au/CQDs composites with or without visible-light irradiation, and the result suggested that a higher amount of HO• was generated by the irradiated sample than that by the nonirradiated one. In the followed control experiments, to further confirm the active oxygen species with radical characteristics, toluene was selected as the substrate in the following experiments. After 12 h of reaction, methyl-group-oxygenated compounds (benzyl alcohol, benzaldehyde, benzoic acid, etc.) were produced in high selectivity of >92%, whereas a mixture of cresols (*o*:*m*:*p* isomer ratio = 2.6:0.8:5.7) was only produced in small amounts (selectivity of <8%, summing the three). Generally speaking, the methyl group

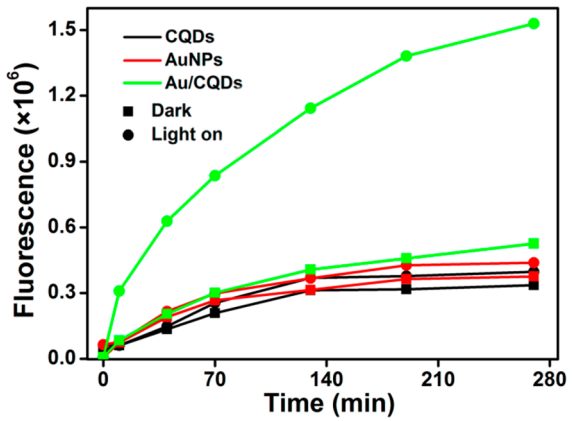

Figure 8. Time dependence of the fluorescence intensity of the supernatant liquid of CQDs, AuNPs, and Au/CQDs composites for two different reaction conditions (in darkness and under visible light). A 450-W xenon lamp was used as the light source with a visible-CUT filter to cut off light with a wavelength of λ < 420 nm.

oxygenation requires abstraction of an H• radical by active oxygen species with radical characteristics.[34,35] The further reactive species trapping experiments were carried out with three different scavengers, *tert*-butanol (a •OH radical scavenger), benzquinamide (BZQ, a O^{2-}• radical scavenger) and disodium ethylenediaminetetraacetate (Na_2-EDTA, a hole scavenger). Figure 7d shows the photocatalytic results after addition of three different scavengers. The addition of *tert*-butanol substantially reduced the photocatalytic activity for the oxidation of cyclohexane from almost 63.8% to 3.3% after 48 h reaction, while the introduction of BZQ and Na_2-EDTA barely affect the photocatalysis results. All of above experiments confirm that that HO• is the active oxygen species in this photocatalytic oxidation process.

dx.doi.org/10.1021/cs400913h | *ACS Catal.* 2014, 4, 328−336

In our present photocatalytic system, as discussed above, the reaction happened in the interface between Au NPs and CQDs. Although the hydroxy radicals have strong oxidation abilities, the synergic effect of the functions of CQDs and the SPR (surface plasmonic resonance) of AuNPs can still protect the products (cyclohexanone and cyclohexanol) from overoxidation.

Tunable-Design Ability of Metal/CQDs Photocatalyst System. The totality of the experiment results suggests the following mechanistic processes in the photocatalytic oxidation of cyclohexane. The surface plasma resonance of AuNPs enhances the light absorption of Au/CQDs composites. Under visible light, H_2O_2 is decomposed to hydroxyl radical (HO•), which serves as a strong oxidant for the conversion of cyclohexane to cyclohexanone. In the process, the interaction between CQDs and AuNPs under visible light plays a key role in the eventual high conversion and selectivity. Based on the proposed mechanism, Ag nanoparticles/CQDs (Ag/CQDs) (see Figure S6 in the Supporting Information) and Cu nanoparticles/CQDs (Cu/CQDs) composite photocatalysts (see Figure S7 in the Supporting Information) were synthesized, and used to catalyze cyclohexane oxidation under the same condition with Au/CQDs system. Like the Au/CQDs system, Ag/CQDs and Cu/CQDs composites exhibited similarly good catalytic performance (see Tables S1 and S2 in the Supporting Information) under purple light (conversion for Ag = 54.0%, selectivity for Ag = 84.1%) and red light (conversion for Cu = 46.7%, selectivity for Cu = 75.3%), which correspond respectively to the surface plasma resonance of Ag nanoparticles (see Figure S6b in the Supporting Information) and Cu nanoparticles (see Figure S7b in the Supporting Information). The results were consistent with the proposed catalytic mechanism discussed above. Therefore, it is possible to tune the wavelength response of the present photocatalyst system based on the surface plasma resonance of metal nanoparticles to achieve high-efficiency and high-selectivity oxidation of cyclohexane, as shown in Figure 9.

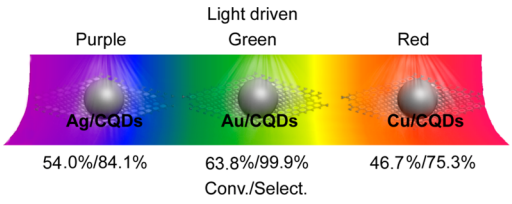

Figure 9. Based on the surface plasma resonance of metal nanoparticles, Ag/CQDs, Au/CQDs, and Cu/CQDs are catalytically active under purple, green, and red light, respectively.

EXPERIMENTAL SECTION

General Information. Unless otherwise noted, all materials including dry solvents were obtained from commercial suppliers and used without further purification. All chemicals were purchased from Sigma–Aldrich. Transmission electron microscopy (TEM) images were recorded using a FEI/Philips Techal 12 BioTWIN TEM operated at 200 kV with EDX analyses. HRTEM images were obtained with a CM200 FEG TEM. UV-vis spectra were measured with an Agilent Model 8453 UV-vis diode array spectrophotometer, while the PL study was conducted with a Horiba Jobin Yvon (FluoroMax 4) luminescence spectrometer. We also collected Raman spectra on a Jobin Yvon Model HR 800 Raman spectroscope (Jobin Yvon, France) equipped with a synapse CCD detector and a confocal Olympus microscope. The spectrograph used 600 g mm^{-1} gratings and a 633 nm He–Ne laser. The crystal structure of the resultant products was characterized by powder X-ray diffraction (XRD) by using an 8/X'Pert-ProMPD (Holand) D/max-γA X-ray diffractometer with Cu Kα radiation (λ = 0.154178 nm). The GC were performed in a Varian 3400 GC column with a cross-linked 5% PhMe silicone column (25 m × 0.20 mm × 0.33 μm) and a FID detector under the following conditions: carrier gas (N_2) at 140 K; temperature program 60 °C, 1 min, 15 °C/min, 180 °C, 15 min; split ratio, 6:1; injector, 280 °C; detector, 280 °C. X-ray absorption near edge structure (XANES) and extended X-ray absorption fine structure (EXAFS) data were collected on Beamline 14W at the Shanghai Synchrotron Radiation Facility. The electrocatalysis action of CQDs was test by a Model CHI 660C workstation (CH Instruments, Chenhua, Shanghai, PRC), while the fluorescence lifetimes of the CQDs were measured using a FluoroLog 3-211-TCSPC system.

General Procedure for Preparation of CQDs. The CQDs were synthesized through a method of electrochemical ablation of graphite. In the synthetic process, two identical graphite rods placed parallel (99.99%, Alfa Aesar Co. Ltd., 13 cm in length and 0.6 cm in diameter) were inserted into the electrolyte at 3 cm above the liquid surface and used as both cathode and anode in a separation distance of 7.5 cm. The electrolyte was ultrapure water (18.4 MΩ cm^{-1}, 600 mL) without any other additives. Static potentials of 15–60 V were applied to the two electrodes using a direct current (DC) power supply for 10 days with intense stirring. Subsequently, a dark-yellow solution appeared gradually in the reactor. The solution was filtered with slow-speed quantitative filter paper, and the resultant solution was centrifuged at 22 000 rpm for 30 min to remove the precipitated graphite oxide and graphite particles. Finally, the obtained solution contained water-soluble CQDs.

General Procedure for Preparation of AuNPs. AuNPs were prepared by chemical reduction method. A aqueous solution (20 mL) containing $HAuCl_4$ (2.5×10^{-4} mol L^{-1}) and trisodium citrate (2.5×10^{-4} mol L^{-1}) were prepared in a conical flask under continuous vigorous stirring. Then ice-cold freshly $NaBH_4$ solution (0.6 mL, 0.1 mol L^{-1}) was added into the above solution. The resultant solution turned pink immediately after adding $NaBH_4$, indicating the formation of AuNPs.

General Procedure for Preparation of Au/CQDs Composites. The Au/CQDs composite was obtained by dropwise addition of $HAuCl_4$ solution (400 μL, 25 mmol L^{-1}) to CQDs solution (20 mL) with vigorous magnetic stirring in a dark environment at room temperature. The resultant mixture was under constant magnetic stirring at room temperature for 2 h, aged overnight, the solution turned red, implying the Au/CQDs composites were obtained. Then, the Au/CQDs composites were centrifuged at 12 000 rpm for 15 min, washed three times with deionized water and ethanol respectively, and finally the obtained sample were dried 6 h at 25–60 °C.

Photoinduced Electron Transfer Properties of CQDs. The PL and photoinduced electron transfer properties of CQDs irradiated by visible light were investigated. In this experiment, PL spectra of the CQDs in organic solutions were recorded with luminescence emission intensities (485 nm excitation, laser source), which were quenched by the known electron acceptors 2,4-dinitrotoluene and electron donors *N*,*N*-diethylaniline in toluene solution (different concentration).

dx.doi.org/10.1021/cs400913h | ACS Catal. 2014, 4, 328–336

The Stern−Volmer quenching constants ($K_{SV} = \tau_F^0 k_q$) were obtained from linear regression. The luminescence decays were tested by TCSPC method. For the CQDs sample, when the excitation wavelength is 485 nm, we monitored the sample with 550 nm narrow bandpass filter, with the observed Stern−Volmer quenching constants ($K_{SV} = \tau_F^0 k_q$) from linear regression.

The Electrocatalytic Activity of Au/CQDs Composites. The electrocatalytic activity of Au/CQDs composites for H_2O_2 decomposition was tested in a conventional three-electrode electrochemical cell with a platinum wire as the auxiliary electrode and an Ag/AgCl (saturated KCl) as the reference electrode. The working electrodes were Au/CQDs composites-modified glassy carbon electrode, The Au/CQDs composites-modified glassy carbon electrode was prepared by spreading aqueous Au/CQDs composites over glassy carbon electrode. A 450-W xenon lamp was used as light source with visible-CUT filter to cut off light with a wavelength of $\lambda < 420$ nm to get visible light, and was positioned 3 cm away from the photoelectrochemical cell. The cyclic voltammograms (CVs) of the bare glassy carbon electrode and Au/CQDs composites over glassy carbon electrode were obtained in 0.05 M phosphate buffer solution (PBS, pH 7.4) in the presence of different H_2O_2 concentration at a scan rate of 25 mV/s. The photocurrent signal was recorded with a Model CHI 660C workstation (CH Instruments, Chenhua, Shanghai, PRC) connected to a personal computer. All electrochemical experiments were carried out at room temperature.

Terephthalic Acid Photoluminescence Probing Assay (TA−PL) To Detect the HO·. Terephthalic acid (THA, 0.415 g), sodium phosphate (Na_3PO_4, 2.2 g), and deionizer water were added into a 250-mL volumetric flask to form a buffer at pH 7.5. After adding a suitable amount of catalyst into the buffer, the mixture was irradiated by visible light or no light. Product fluorescence (THA−OH) was measured with a fluorescent spectrophotometry (Horiba Jobin Yvon, FluoroMax 4) with 350 nm excitation and 429 nm emission at pH 7.5.

CONCLUSIONS

In conclusion, we report that the Au/CQDs composite shows unprecedentedly high photocatalytic activity for the selective oxidation of cyclohexane to cyclohexanone with a conversion efficiency of 63.8% and a selectivity of over 99.9% using H_2O_2 as oxidant without any solvents. The mechanism of the catalyst system is proposed to involve: enhancement of light absorption by surface plasma resonance of metal nanoparticles, production of active oxygen species (HO·) by H_2O_2 decomposition, and interaction between CQDs and AuNPs under visible light; these processes collectively lead to the eventual high conversion and selectivity. The present work suggests a new route for the design of high-performance photocatalytic systems for selective hydrocarbon oxidation for green chemical industry.

ASSOCIATED CONTENT

Supporting Information

UV-vis spectra and (HR)TEM images of metal nanoparticles/CQDs composites. This material is available free of charge via the Internet at http://pubs.acs.org.

AUTHOR INFORMATION

Corresponding Authors

*E-mail: yangl@suda.edu.cn (Y. Liu).
*E-mail: zhkang@suda.edu.cn (Z. Kang).

Notes

The authors declare no competing financial interest.

ACKNOWLEDGMENTS

This work is supported by the National Basic Research Program of China (973 Program) (Nos. 2012CB825800 and 2013CB932702), the National Natural Science Foundation of China (Nos. 51132006, 21073127, and 21071104), the Specialized Research Fund for the Doctoral Program of Higher Education (No. 20123201110018), a Suzhou Planning Project of Science and Technology (No. ZXG2012028), a Foundation for the Author of National Excelent Doctoral Dissertation of China (No. 200929), and a project funded by the Priority Academic Program Development of Jiansu Higher Education Institutions.

REFERENCES

(1) Schuchardt, U.; Cardoso, D.; Sercheli, R.; Pereira, R.; da Cruz, R. S.; Guerreiro, M. C.; Mandelli, D.; Spinacé, E. V.; Pires, E. L. *Appl. Catal., A* **2001**, *211*, 1−17.
(2) Cao, Y. H.; Yu, H.; Tan, J.; Peng, F.; Wang, H. J.; Li, J.; Zheng, W. X.; Wong, N.-B. *Carbon* **2013**, *57*, 433−442.
(3) Bromberg, S. E.; Yang, H.; Asplund, M. C.; Lian, T.; McNamara, B. K.; Kotz, K. T.; Yeston, J. S.; Wilkens, M.; Frei, H.; Bergman, R. G.; Harris, C. B. *Science* **1997**, *278*, 260−263.
(4) Hattori, H.; Ide, Y.; Ogo, S.; Inumaru, K.; Sadakane, M.; Sano, T. *ACS Catal.* **2012**, *2*, 1910−1915.
(5) Wang, C. H.; Chen, L. F.; Qi, Z. W. *Catal. Sci. Technol.* **2013**, *3*, 1123−1128.
(6) Bonnet, D.; Ireland, T.; Fache, E.; Simonato, J.-P. *Green Chem.* **2006**, *8*, 556−559.
(7) Hamdy, M. S.; Ramanathan, A.; Maschmeyer, T.; Hanefeld, U.; Jansen, J. C. *Chem.—Eur. J.* **2006**, *12*, 1782−1789.
(8) Pillai, U.; Sahle-Demessie, R. E. *Chem. Commun.* **2002**, *0*, 2142−2143.
(9) Chavez, F. A.; Nguyen, C. V.; Olmstead, M. M.; Mascharak, P. K. *Inorg. Chem.* **1996**, *35*, 6282−6291.
(10) Comba, P.; Maurer, M.; Vadivelu, P. *Inorg. Chem.* **2009**, *48*, 10389−10396.
(11) Goldstein, A. S.; Beer, R. H.; Drago, R. S. *J. Am. Chem. Soc.* **1994**, *116*, 2424−2429.
(12) Yiu, S.-M.; Man, W.-L.; Lau, T.-C. *J. Am. Chem. Soc.* **2008**, *130*, 10821−10827.
(13) Pârvulescu, V. I.; Dumitriu, D.; Poncelet, G. *J. Mol. Catal. A—Chem.* **1999**, *140*, 91−105.
(14) Spinacé, E. V.; Pastore, H. O.; Schuchardt, U. *J. Catal.* **1995**, *157*, 631−635.
(15) Lü, G. M.; Ji, D.; Qian, G.; Qi, Y. X.; Wang, X. L.; Suo, J. S. *Appl. Catal., A* **2005**, *280*, 175−180.
(16) Raja, R.; Sankar, G.; Thomas, J. M. *J. Am. Chem. Soc.* **1999**, *121*, 11926−11927.
(17) Yuan, Y.; Ji, H. B.; Chen, Y. X.; Han, Y.; Song, X. F.; She, Y. B.; Zhong, R. G. *Org. Process Res. Dev.* **2004**, *8*, 418−420.
(18) Sarkar, B.; Prajapati, P.; Tiwari, R.; Tiwari, R.; Ghosh, S.; Acharyya, S. S.; Pendem, C.; Singha, R. K.; Konathala, L. N. S.; Kumar, J.; Sasaki, T.; Bal, R. *Green Chem.* **2012**, *14*, 2600−2606.
(19) Baker, S. N.; Baker, G. A. *Angew. Chem., Int. Ed.* **2010**, *49*, 6726−6744.
(20) Li, H. T.; Liu, R. H.; Lian, S. Y.; Liu, Y.; Huang, H.; Kang, Z. H. *Nanoscale* **2013**, *5*, 3289−3297.
(21) Li, H. T.; He, X. D.; Kang, Z. H.; Huang, H.; Liu, Y.; Liu, J. L.; Lian, S. Y.; Tsang, C. H. A.; He, X. D.; Lee, S.-T. *Angew. Chem., Int. Ed.* **2010**, *49*, 4430−4434.
(22) Wittstock, A.; Zielasek, V.; Biener, J.; Friend, C. M.; Bäumer, M. *Science* **2010**, *327*, 319−322.

(23) Gu, J. L.; Gu, Y. L.; Huang, Y.; Elangovan, S. P.; Li, Y. S.; Zhao, W. R.; Toshio, I.; Yamazaki, Y.; Shi, J. L. *J. Phys. Chem. C* **2011**, *115*, 21211−21217.
(24) Shimizu, K.-I.; Murata, Y.; Satsuma, A. *J. Phys. Chem. C* **2007**, *111*, 19043−19051.
(25) Shankar, S. S.; Rai, A.; Ahmad, A.; Sastry, M. *J. Colloid Interface Sci.* **2004**, *275*, 496−502.
(26) Li, H. T.; Kang, Z. H.; Liu, Y.; Lee, S.-T. *J. Mater. Chem.* **2012**, *22*, 24230−24253.
(27) Baruah, B.; Craighead, C.; Abolarin, C. *Langmuir* **2012**, *28*, 15168−15176.
(28) Ming, H.; Ma, Z.; Liu, Y.; Pan, K. M.; Yu, H.; Wang, F.; Kang, Z. H. *Dalton Trans.* **2012**, *41*, 9526−9531.
(29) Luo, P. H.; Li, C.; Shi, G. Q. *Phys. Chem. Chem. Phys.* **2012**, *14*, 7360−7366.
(30) Li, J.; Shi, Y.; Xu, L.; Lu, G. Z. *Ind. Eng. Chem. Res.* **2010**, *49*, 5392−5399.
(31) Jiang, D. T.; Sham, T. K.; Norton, P. R. *Phys. Rev. B* **1994**, *49*, 3709−3712.
(32) Zhang, P.; Sham, T. K. *Phys. Rev. Lett.* **2003**, *90*, 245502.
(33) Miyake, T.; Hamada, M.; Sasaki, Y.; Oguri, M. *Appl. Catal., A* **1995**, *131*, 33−42.
(34) Kang, Z. H.; Wang, N. B.; Mao, B. D.; Su, Z. M.; Gao, L.; Niu, L.; Shan, H. Y.; Xu, L. *Appl. Catal., A* **2006**, *299*, 212−217.
(35) Niwa, S.-I.; Eswaramoorthy, M.; Nair, J.; Raj, A.; Itoh, N.; Shoji, H.; Namba, T.; Mizukami, F. *Science* **2002**, *295*, 105−107.